Research Article

Francisco J. Betancourt, Jonathan Rincón Saucedo, Fidel Flores-Ocampo, Francisco V. Flores-Baez, Antonio Paz, and José Rubén Morones-Ibarra*

QCD phase diagram in a finite volume in the PNJL model

https://doi.org/10.1515/phys-2022-0039
received March 02, 2022; accepted April 11, 2022

Abstract: In this work, we study the quantum chromodynamics phase diagram at finite temperature and non-zero chemical potential in the framework of the SU(2) flavor of the Polyakov–Nambu – Jona–Lasinio model (PNJL). Applying multiple reflection expansion to cubic and spherical finite volumes of different sizes and boundary conditions, the chiral phase transition and deconfinement of strongly interacting matter are analyzed. We give special attention to find and locate the critical endpoint and locating the critical endpoint, if it exists, as a function of the volume size and its shape, and its dependence of chemical potential and temperature.

Keywords: polyakov Nambu–Jona–Lasinio model, critical end point, chiral phase transition, multiple reflection expansion, QCD effective theories

1 Introduction

Confinement and the spontaneous breaking of chiral symmetry are two of the main characteristics of quantum chromodynamics (QCD) [1–3]. A system of strongly interacting particles undergoes a phase transformation when it is subject to high temperatures and/or high densities. Quarks deconfinement and/or restoration of chiral symmetry can occur under these extreme conditions [4–7]. These phase transformations are the subject of an intense research activity at present time due to the importance of this phenomenon in modern physics. The study of QCD phase diagrams has attracted a lot of attention in recent years due to the experimental projects in progress and the improved lattice QCD techniques and non-perturbative methods at finite temperature and chemical potential [8,9].

The topic of QCD phase transition is important in several fields of modern physics. In cosmology, for example, it is involved in the processes that happened in the early Universe. In astrophysics, it is important to understand the states of matter in the compact stars [10]. In high-energy physics and nuclear physics, the knowledge of the processes that occur in relativistic heavy ion collisions requires the study of strongly interacting systems subject to conditions of very high temperatures and density [11].

The exotic state of matter can be formed in heavy ion collisions. One of the main investigation lines in theoretical and experimental physics is to understand the properties of these new states of matter [12] subject to extreme conditions, studying their phase diagrams at finite temperature and chemical potentials. This is a topic of increasing interest being researched in experiments such as the ones taking place in the relativistic heavy ion collider and in the large hadron collider, from which they expected to get important information about the phases of strongly interacting matter. There are several important questions in the study of QCD phase transitions that we address in this work. One of them is to determine the existence and the location of the critical endpoint (CEP) in the chiral phase diagram [11,13,14]. For the case of current quark masses different from zero, the CEP is a point in the temperature–density ($\mu - T$) plane, where the nature of the transition phase changes from a smooth crossover to a first-order transition. In the case of chiral limit, we look for a tricritical point (TCP), which will be located at the end of a first-order transition, where a line of second-order phase transition starts.

In a confinement/deconfinement phase diagram, a CEP is expected to appear in the point where the line of a first-order transition undergoes a change to a crossover region. We have found that the location of the CEP is

* Corresponding author: José Rubén Morones-Ibarra, CICFIM-Facultad de Ciencias Físico-Matemáticas, Universidad Autónoma de Nuevo León, San Nicolás de los Garza, Nuevo León, 66455, México, e-mail: rubenmorones@yahoo.com.mx
Francisco J. Betancourt, Jonathan Rincón Saucedo, Fidel Flores-Ocampo, Francisco V. Flores-Baez, Antonio Paz: CICFIM-Facultad de Ciencias Físico-Matemáticas, Universidad Autónoma de Nuevo León, San Nicolás de los Garza, Nuevo León, 66455, México

sensible to several conditions such as the size of the system, the geometry of the volume enclosing it, and the boundary conditions used in the model [15].

In our study of the phase transition between hadronic matter and quark-gluon plasma, as well as the chiral phase transition, the influence of finite volume in the location of CEP and in the quark effective mass is studied for a cubic volume with multiple reflection expansion (MRE) approximation.

The Polyakov–Nambu – Jona–Lasinio (PNJL) model involves chiral symmetry breaking and confinement at low energies, which are two of the main characteristic of QCD. We calculate the thermodynamic potential at finite volume on the framework of the SU(2) flavor version of the PNJL model. To take into account the effects of finite volumes in the model, we calculate the density of states by using the multiple reflection expansion approximation [16–21].

In ref. [17], this method was used to study the Nambu–Jona–Lasinio (NJL) model in SU(2) with a spherical volume of radius R. In our work, we make an extension of the NJL model toward the PNJL model at finite volume using the same idea. We study how the behavior of the order parameters changes in a finite volume with different sizes, shapes, and boundary conditions. Likewise, we report the existence or absence of the CEP and its location on the temperature–density ($\mu - T$) plane.

2 PNJL model

The NJL model is a good prospect to study systems of strongly interacting matter at finite temperature and chemical potential. One of the drawbacks of this model is that it does not take into account the property of confinement. The interaction between quarks is introduced as point-like interactions and does not include gluon exchange. A way to go around this limitation is by introducing the Polyakov loop to construct a more complete model that takes into account the confinement of quarks at low energies [22–24].

We start with the two flavor quark version of the NJL model including the Polyakov loop for three colors with the Lagrangian given by ref. [24]

$$\begin{aligned}\mathscr{L}_{\text{PNJL}} &= \bar{q}[i\gamma^{\mu}D_{\mu} - m_o + \gamma_o\mu]q \\ &\quad + \frac{G}{2}[(\bar{q}q)^2 + (\bar{q}i\gamma_5\boldsymbol{\tau}q)^2] - \mathcal{U}(\varphi, \varphi^*; T),\end{aligned} \tag{1}$$

where m_o is the current quark mass and we assume isospin symmetry, i.e., $m_u = m_d = m_o$. The covariant derivative $D_{\mu} = \partial_{\mu} - iA_{\mu}$ introduces an extern gluonic field A_{μ}, which interacts with the quarks. This gluonic field $A_{\mu}(A_o, \boldsymbol{A})$ is produced by a very heavy quark, which means that it has no dynamics properties. This means that the dynamic part represented by $\boldsymbol{A}$ is not taken into account so that only the part associated with the potential of the field remains. The thermodynamic potential per unit volume, $\Omega(T, \mu) = -T \ln Z/V$, is used to calculate the thermodynamic properties. Here, the partition function Z is expressed as follows:

$$Z = \int D\bar{q}Dq\ e^{i\int d^4x\,\mathscr{L}_{\text{PNJL}}}, \tag{2}$$

and then, the thermodynamic potential after using mean field approximation is expressed as follows:

$$\begin{aligned}\Omega_{\text{PNJL}} &= \mathcal{U}(\varphi, \varphi^*; T) + \frac{(M - m_o)^2}{4G} \\ &\quad - 2N_fN_c\int\frac{d^3\boldsymbol{p}}{(2\pi)^3}\{E_{\boldsymbol{p}} + T \\ &\quad \times [\ln(1 + L^{\dagger}e^{-\beta(E-\mu)}) + \ln(1 + e^{-\beta(E+\mu)}L)]\},\end{aligned} \tag{3}$$

where

$$L(\boldsymbol{x}) = Pe^{i\int_o^{\beta}A_4\mathrm{d}\tau} = e^{i\beta A_4} \tag{4}$$

is the Wilson line, a matrix in color space which, when written as a diagonal matrix, represents a complex field called the Polyakov loop [1,2,21,25,26]:

$$\Phi(\boldsymbol{x}) = \frac{1}{3}\mathrm{Tr}[L(\boldsymbol{x})]; \quad \Phi^*(\boldsymbol{x}) = \frac{1}{3}\mathrm{Tr}[L^{\dagger}(\boldsymbol{x})]. \tag{5}$$

The expression $\mathcal{U}(\Phi, \Phi^*)$ of Eq. (1) is the potential associated with the Polyakov loop. There are several proposals for this Polyakov loop potential $\mathcal{U}$, such as polynomial, exponential, and logarithmic expressions [13,29,30]. In this work, we use the polynomial potential, as mentioned in study by Fukushima [13]:

$$\mathcal{U} = T^4\left(-\frac{b_2(T)}{2}\Phi\Phi^* - \frac{b_3}{6}(\Phi^3 + \Phi^{*3}) + \frac{b_4}{4}(\Phi\Phi^*)^2\right), \tag{6}$$

where

$$b_2 = a_0 + a_1\frac{T_0}{T} + a_2\left(\frac{T_0}{T}\right)^2 + a_3\left(\frac{T_0}{T}\right)^3, \tag{7}$$

with parameters $a_0 = 6.76$, $a_1 = -1.95$, $a_2 = 2.625$, $a_3 = -7.44$, $T_0 = 270$ MeV, $b_3 = 0.75$, and $b_4 = 7.5$. These values were used to reproduce the results obtained in lattice QCD [13,29].

The field $A_{\mu} = A_{\mu}^a T^a$ comes from the generators $T^a = \lambda^a/2$ of the gauge transformation SU(3), $U = e^{ig\varepsilon_a T^a}$, where λ^a are the zero-trace Gell-Mann matrices with $a = 1, \ldots, 8$. A set of

SU(3) transformations $U_c = \{\mathrm{I}, e^{i2\pi/3}, e^{i4\pi/3}\}_{3\times3}$ that preserve periodic boundary conditions in the gluon field must commute with all the $A_\mu(\boldsymbol{x}, \tau)$ matrices of the SU(3) and is the group called center symmetry group $Z(3) \in \mathrm{SU}(3)$. As this symmetry appears only in an Euclidean space where we have periodic conditions for A_μ, then, for dynamic quarks, this symmetry does not exist. As the presence of the Polyakov loop destroys the symmetry, the condition to maintain it is that $\Phi(\boldsymbol{x}) = 0$ [31]; any non-zero value implies broken symmetry, and then, the Polyakov loop can be considered an order parameter for the transition from the confinement to the unconfinement phase. In particular, $\Phi(\boldsymbol{x})$ is gauge invariant, but it is not center symmetry invariant, so this invariance or change is interpreted as the free energy of an external static color charge source that is added to the system. This color charge must be introduced in a way that preserves the gauge invariance, and the Wilson line Eq. (4) in the direction of time is the most efficient way to do this. In this way, defining the Polyakov loop as $\Phi(x) = e^{-\beta F}$, where F is the free energy of a test quark, it follows that in the confinement phase of a theory in which the free energy to add a source of color charge must be infinite, then Φ must be zero [32].

The constituent quark mass M, or dynamically generated mass, is obtained from the minimization of the thermodynamic potential, Eq. (3), $\partial\Omega/\partial\sigma = 0$, from which the gap equation is obtained:

$$M - m_o - 4GN_cN_f \int \mathrm{d}p \frac{p^2}{2\pi^2}\frac{M}{E_p}[1 - g^{(+)} - g^{(-)}] = 0, \quad (8)$$

where the functions $g^{(+)}$ and $g^{(-)}$ are

$$g^{(+)} = \frac{\Phi e^{-\beta(E+\mu)} + 2\Phi^* e^{-2\beta(E+\mu)} + e^{-3\beta(E+\mu)}}{1 + 3\Phi e^{-\beta(E+\mu)} + 3\Phi^* e^{-2\beta(E+\mu)} + e^{-3\beta(E+\mu)}} \quad (9)$$

$$g^{(-)} = \frac{\Phi^* e^{-\beta(E-\mu)} + 2\Phi e^{-2\beta(E-\mu)} + e^{-3\beta(E-\mu)}}{1 + 3\Phi^* e^{-\beta(E-\mu)} + 3\Phi e^{-2\beta(E-\mu)} + e^{-3\beta(E-\mu)}}, \quad (10)$$

and the mass M is related to the quark condensate $\langle\bar{q}q\rangle \approx -\sigma/2G$ by [33,34]:

$$M = m_o - 2G\langle\bar{q}q\rangle. \quad (11)$$

In the same way, imposing equilibrium conditions minimizing the thermodynamic potential, equations for Φ and Φ^* are obtained, so, from the system of equations,

$$\frac{\partial\Omega}{\partial\sigma} = 0; \quad \frac{\partial\Omega}{\partial\Phi} = 0; \quad \frac{\partial\Omega}{\partial\Phi^*} = 0, \quad (12)$$

it is possible to obtain the mass and the expectation values of the Polyakov loop with T and μ as parameters [2].

3 Finite volume

To determine the effects of a finite volume in the QCD phase structure in the PNJL model, we follow the idea proposed by Kiriyama *et al.* [17] who used the MRE approximation to include the density of states for a spherical volume in a NJL model for SU(2). In this section, we extend this case to the PNJL model in the same SU(2) framework to study how the states of chiral symmetry and confinement behave in a finite volume.

3.1 Spherical volume

Following ref. [17], we redefine the density of states $\rho = \frac{d^3\boldsymbol{p}}{(2\pi)^3}$ as a density of MRE states ρ_{MRE} [16,20], which restrict the system to a spherical volume of radius R. The density of states in a spherical droplet model is composed of three terms: the volumetric density, the surface density, and the curvature contribution, given by

$$\rho_{\mathrm{MRE}} = \rho_{\mathrm{vol}} + \rho_{\mathrm{surf}} f_S + \rho_{\mathrm{curv}} f_C, \quad (13)$$

$$\rho_{\mathrm{MRE}} = \frac{p^2}{2\pi^2}\left[1 + \frac{6\pi^2}{pR}f_S + \frac{12\pi^2}{(pR)^2}f_C\right], \quad (14)$$

where both the surface and curvature terms are a function of the momentum p and α parameters:

$$f_S\left(\frac{p}{\alpha}\right) = -\frac{1}{8\pi}\left[1 - \frac{2}{\pi}\arctan\frac{p}{\alpha}\right] \quad (15)$$

$$f_C\left(\frac{p}{\alpha}\right) = \frac{1}{12\pi^2}\left[1 - \frac{3p}{2\alpha}\left(\frac{\pi}{2} - \arctan\frac{p}{\alpha}\right)\right]. \quad (16)$$

To handle definitions (15) and (16) numerically, Dirichlet and Neumann boundary conditions are imposed on the α parameter [17,20].

For Dirichlet conditions, we make $\alpha \to \infty$, and then,

$$\lim_{\alpha\to\infty} f_S\left(\frac{p}{\alpha}\right) = -\frac{1}{8\pi} \quad (17)$$

$$\lim_{\alpha\to\infty} f_C\left(\frac{p}{\alpha}\right) = \frac{1}{12\pi^2}. \quad (18)$$

For Neumann boundary conditions, we establish $\alpha \to 0$, so

$$\lim_{\alpha\to0} f_S\left(\frac{p}{\alpha}\right) = 0, \quad (19)$$

$$\lim_{\alpha\to0} f_C\left(\frac{p}{\alpha}\right) = -\frac{1}{24\pi^2}. \quad (20)$$

In this way, the final expression of the integral in Eq. (8) can be written as follows:

$$\int \mathrm{d}p \frac{p^2}{2\pi^2} f(T,\mu,\boldsymbol{p}) \longrightarrow \int_0^{\infty} \mathrm{d}p\ \rho(p) f(T,\mu,p) \tag{21}$$

$$\longrightarrow \int_{\Lambda_{\mathrm{IR}}}^{\Lambda_{\mathrm{UV}}} \mathrm{d}p\ \rho_{\mathrm{MRE}}(p,\alpha,R) f(T,\mu,p), \tag{22}$$

where Λ_{UV} is the tri-momentum cutoff, which works as the upper limit of the integral for purposes of regularization. By imposing these conditions, we obtain the densities of states for Dirichlet and Neumann conditions:

$$\rho_{\mathrm{MRE}} = \frac{p^2}{2\pi^2}\left[1 - \frac{3\pi}{4pR} + \frac{1}{(pR)^2}\right], \tag{23}$$

$$\rho_{\mathrm{MRE}} = \frac{p^2}{2\pi^2}\left[1 - \frac{1}{2(pR)^2}\right]. \tag{24}$$

The density of states (14) has an intrinsic physical limit for momentum values since it is quadratic and therefore has a range of negative momentum values that are not physically acceptable. This imposes a lower limit Λ_{IR} in the solution of Eqs. (23) and (24). This value is set to $\Lambda_{\mathrm{IR}} = 1.8/R$ for the Dirichlet conditions and $\Lambda_{\mathrm{IR}} = (R\sqrt{2})^{-1}$ for the Neumann conditions.

3.2 Cubic volume

There are several ways to study the problem with finite volume. In some of them, it is solved by establishing boundary conditions so that the shape of the region with finite volume is not relevant; in others, the geometry is important, and we can study the effect, for example, of using spherical or cubic volumes. In the previous analysis, the density of MRE states imposes the condition of finite volume and in particular that of a form of spherical droplets.

Adding boundary conditions to the PNJL model makes it more expensive, computationally speaking, so considering that the MRE approach should be simple to implement, and although we know that MRE approximation is designed to describe spheres, in this section, we will extend it in a rough approximation to a cubic box shape by making two simple changes to the ρ_{MRE}. We first redefine the surface term ρ_{surf} to consider the surface of a cube with edge L and further establish that the curvature factor f_C is zero. In this way, we build ρ_{MRE} that approximates a cube shape. Our purpose is to show whether it is still a good approximation for a finite volume that, in addition to chiral symmetry, includes deconfinement and that it is simple to implement.

As mentioned in Eq. (14), the density of states is composed of three terms, and since in Eq. (3) the integrand is spherically symmetric, we can use the relation $\mathrm{d}N_v = V\mathrm{d}\boldsymbol{p}/(2\pi)^3$, which leads to $\mathrm{d}\boldsymbol{p} = 4\pi p^2 \mathrm{d}p$ in the first two terms of Eq. (13) to obtain the volumetric density of states:

$$\rho_{\mathrm{vol}} = \frac{1}{V}\frac{\mathrm{d}N_v}{\mathrm{d}p} = \frac{p^2}{2\pi^2}. \tag{25}$$

By analogy with the volumetric density of states, the surface density of states is $\mathrm{d}N_s = Ad^2\boldsymbol{p}/(2\pi)^2$, where A represents the area of the six faces of a cube with edge L, that is, $A = 6L^2$. Thus, we can obtain $d^2\boldsymbol{p} = 2\pi p \mathrm{d}p$, then the surface term of Eq. (13) will be

$$\left(\frac{\mathrm{d}N_s}{\mathrm{d}p}\right) f_S = \frac{Ap}{2\pi}\left(-\frac{1}{8\pi}\right) = -\frac{6L^2Lp}{16L\pi^2}. \tag{26}$$

Setting $f_C = 0$ for the curvature factor in Eq. (13) and using Eqs. (25) and (26), after making $\rho = \frac{1}{V}\frac{\mathrm{d}N}{\mathrm{d}p}$, the expression for the density of states is

$$\rho_{\mathrm{MRE}} = \frac{p^2}{2\pi^2}\left[1 - \frac{3}{4Lp}\right], \tag{27}$$

where L is the length of the cube's edge. To avoid unphysical features of the model, the interval between $p = 0$ and $p = 3/4L$ is not taken into account, and the greatest root is set as an infrared cutoff $\Lambda_{\mathrm{IR}} = 3/4L$.

4 Model parameters

This PNJL model was regularized by using the tri-momentum cutoff scheme, and like any other regularization scheme, it needs two parameters: the coupling strength G and a tri-momentum cutoff Λ_{UV} [35]. In addition, a third parameter, the infrared cutoff Λ_{IR}, arises from implementation of the MRE approximation. The values we used were those obtained by ref. [29] for a bare quark mass $m_o = 5.5$ MeV and mass and decay constant of pion of $m_\pi = 139$ MeV and $f_\pi = 92.3$ MeV, respectively, and a value for the quark condensate of $\langle \bar{u}u \rangle^{1/3} = 251$ MeV. The values of the regularization parameters are then found to be $\Lambda = 651$ MeV and $G = 10.08 \times 10^{-6}$ MeV^{-2}.

5 Zero-μ

5.1 Order parameters: sphere and cubic box

At the chiral limit, $m_o = 0$, and considering the case where $\mu = 0$, curves for the dynamical mass M and the

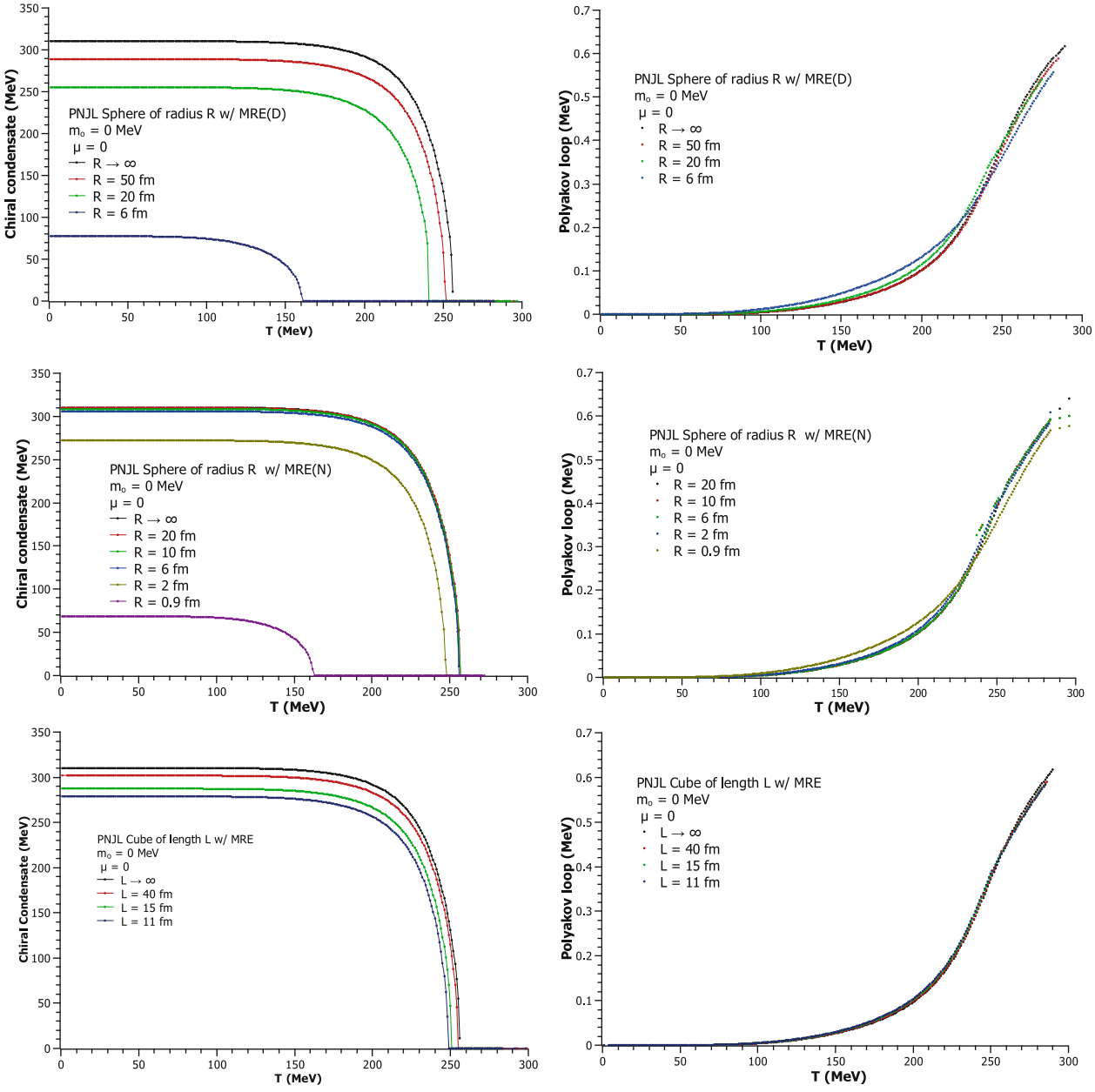

Figure 1: Comparison of the behavior of the order parameter as a function of temperature for the PNJL model with MRE approximation in sphere and cubic shapes with different volumes and $m_0 = 0$ MeV. Left side, the quark condensate $\langle \bar{q}q \rangle$. Right side, the Polyakov loop. Above, sphere of radius R and Dirichlet conditions; center, sphere of radius R and Neumann conditions; bottom, cube of edge L.

Polyakov loop Φ, both as functions of T, show a characteristic behavior. Zero values in the order parameter M imply restoration of chiral symmetry. Nonzero values in the Polyakov loop Φ imply deconfinement. Figure 1 shows the behavior of both $\langle \bar{q}q \rangle$ and Φ order parameters for the PNJL model at finite volume using the MRE approximation for different sizes of sphere and cubic volumes in the chiral limit $m_o = 0$. For both geometries, a phase transition from the second to the first-order is observed for $\mu = 0$.

Unlike the cube, which shows similar values in the constituent mass M for different volume sizes, there is considerable variation in the value of this M as the volume of the sphere decreases. Similarly, for the sphere, it is observed that the phase changes, as the volume decreases, occur at well-spaced T values, while for the cube, these changes occur in a small interval of temperatures. In general, as expected, decreasing the size of the volume size shifts the chiral phase transition to lower values of T.

On the other hand, the Polyakov loop, at the right of Figure 1, shows a rapid phase transition for both sphere and cube, and practically no difference is observed when the volume size or the geometry are modified.

When the current mass of quarks is $m_o = 5.5$ MeV, the chiral crossover transition is observed in both geometries as shown in Figure 2. The behavior of the constituent mass is similar to that observed in the chiral limit where it is evident that, for a cubic geometry, this parameter is not very sensitive to changes in the volume.

Table 1 summarizes the constituent masses calculated in the chiral limit for different volumes of a sphere, with both Dirichlet and Neumann boundary conditions, and different volumes of a cube, and in Table 1, the constituent masses for the same geometries when the current quark mass is $m_o = 5.5$ MeV are shown.

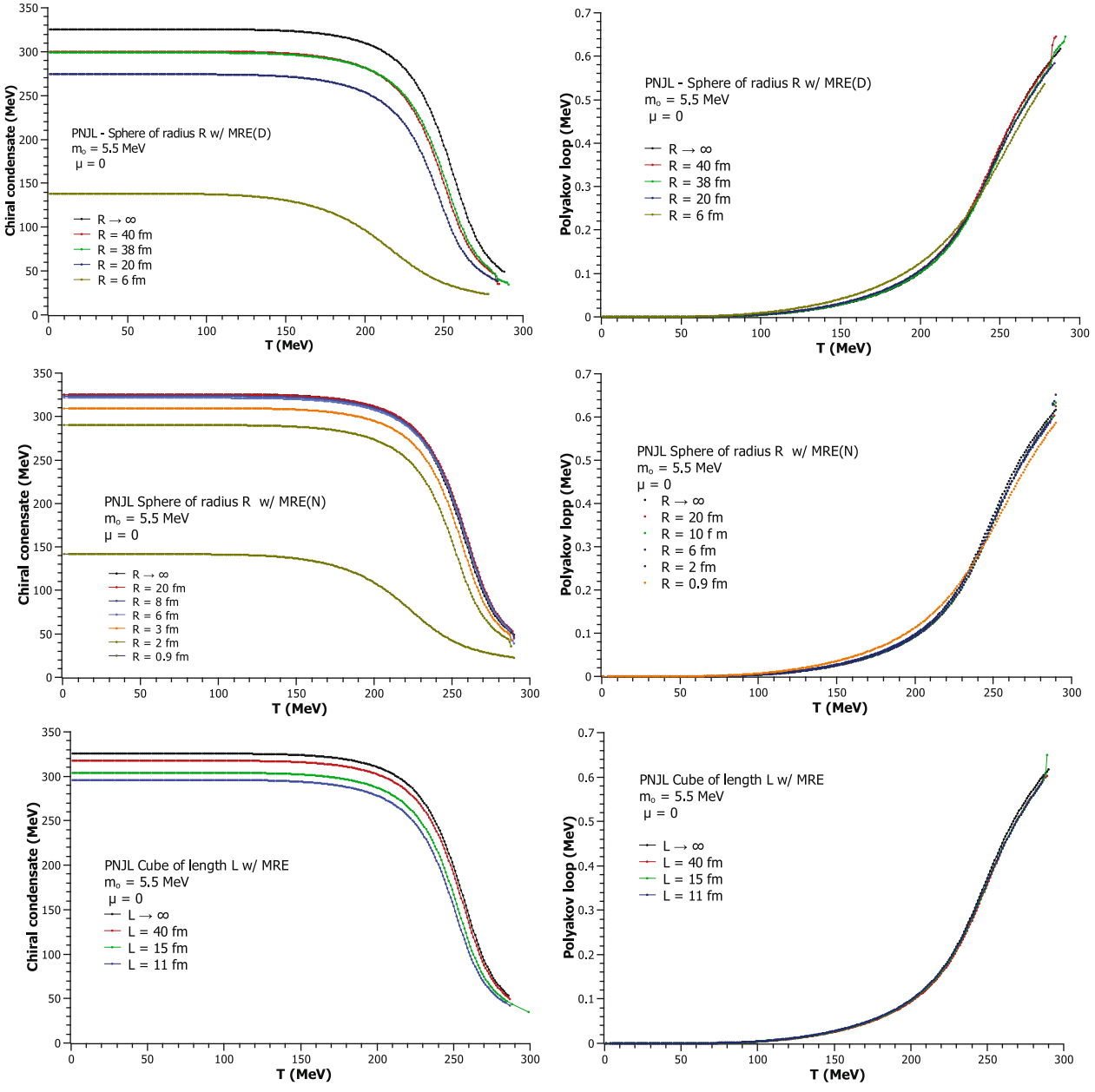

Figure 2: Comparison of the behavior of the order parameter as a function of temperature for the PNJL model with MRE approximation in sphere and cubic shapes with different volumes and $m_0 = 5.5$ MeV. Left side, the quark condensate $\langle \bar{q}q \rangle$. Right side, the Polyakov loop. Above, sphere of radius R and Dirichlet conditions; center, sphere of radius R and Neumann conditions; bottom, cube of edge L.

Table 1: Top, constituent mass in the quiral limit using the PNJL model in a finite volume, for different sizes and geometries and bottom constituent mass for $m_0 = 5.5$ MeV

PNJL MRE_D sphere		PNJL MRE_N sphere		PNJL MRE cube	
$m_o = 0$		$m_o = 0$		$m_o = 0$	
R (fm)	M (MeV)	R (fm)	M (MeV)	L (fm)	M (MeV)
50	288.78	20	309.81	40	301.74
20	255.19	10	308.63	15	287.30
10	193.18	6	305.88	13	283.68
6	77.35	2	272.13	11	278.69
		0.9	68.40	9	271.39
				5	237.63
PNJL MRE_D sphere		PNJL MRE_N sphere		PNJL MRE cube	
$m_o = 5.5$ MeV		$m_o = 5.5$ MeV		$m_o = 5.5$ MeV	
R (fm)	M (MeV)	R (fm)	M (MeV)	L (fm)	M (MeV)
50	305.33	20	325.15	40	317.52
40	300.21	10	324.04	15	303.94
38	298.86	8	323.22	13	300.55
20	274.15	6	321.46	11	295.90
10	219.16	4	316.49	9	289.11
6	138.1	3	309.61	5	258.20
		2	290.12		
		0.9	141.55		

6 Finite-μ

6.1 Order parameters

As expected, when the chemical potential μ is different from zero, the order parameters behave differently. Figure 3 shows the behavior of a sphere of radius $R = 38$ fm using the MRE_D approximation. As the value of μ increases, the order parameter curve (left side) changes so that the inflection point of the curve obtained shifts through a wide arrange of values of T. An abrupt rise occurs ($T \approx 25$ MeV) in this curve ($\mu = 326$ MeV) and then continues to show a smooth curve pattern ($\mu = 336$ MeV). This behavior is a clear sign of a change in the type of phase transition, which is associated with the existence and the location of the CEP. Curves for the Polyakov loop are shown on the right side of the figure: for values of μ smaller than 326 MeV, the chiral phase transition is a crossover; larger values in μ are first-order transitions. Similar cases for a sphere_N of $R = 6\ fm$ and cube of $L = 13\ fm$ are shown in the center and below, respectively.

6.2 Susceptibilities

Susceptibility is the response of the potential to changes in the order parameters [24,36]. It can be used to study phase transitions, as divergences in susceptibility are associated with phase changes.

As ref. [26] says, when establishing the PNJL model, we have a model based on a chiral symmetry that compensates for the lack of confinement through the Polyakov loop. With this PNJL model, we can compare the temperatures at which deconfinement and restoration of chiral symmetry occur, and assuming that both processes occur at the same temperature, a susceptibility matrix can be defined as follows:

$$\chi = \begin{pmatrix} \chi_{MM} & \chi_{M\Phi} & \chi_{M\Phi^*} \\ \chi_{\Phi M} & \chi_{\Phi\Phi} & \chi_{\Phi\Phi^*} \\ \chi_{\Phi^* M} & \chi_{\Phi^*\Phi} & \chi_{\Phi^*\Phi^*} \end{pmatrix}^{-1}, \tag{28}$$

where its components are the second derivatives of the thermodynamic potential Ω with respect to the order parameters M, Φ, and Φ^*

$$\begin{aligned} \chi_{MM} &= \frac{1}{T\Lambda}\partial_{MM}\Omega; \quad \chi_{M\Phi} = \frac{1}{T\Lambda^2}\partial_{M\Phi}\Omega \\ \chi_{\Phi\Phi} &= \frac{1}{T\Lambda^3}\partial_{\Phi\Phi}\Omega; \quad \chi_{\Phi\Phi^*} = \frac{1}{T\Lambda^3}\partial_{\Phi\Phi^*}\Omega \\ \chi_{\Phi^*\Phi^*} &= \frac{1}{T\Lambda^3}\partial_{\Phi^*\Phi^*}\Omega; \quad \chi_{\Phi^* M} = \frac{1}{T\Lambda^2}\partial_{\Phi^* M}\Omega. \end{aligned} \tag{29}$$

We define χ_{MM} as the chiral susceptibility. Likewise, an observable associated with the Polyakov loop is shown in ref. [2], and the average Polyakov loop susceptibility is defined as follows:

$$\overline{\chi}_{\Phi\Phi} = \frac{1}{4}[\chi_{\Phi\Phi} + \chi_{\Phi^*\Phi^*} + 2\chi_{\Phi\Phi^*}]. \tag{30}$$

6.3 Chiral and loop susceptibilities for a finite volume

Peaks in susceptibility indicate changes in the phase of the model. These occur at T_{ch} and T_d for chiral susceptibility and average Polyakov loop susceptibility, respectively. Figure 4 shows both chiral and average Polyakov loop susceptibility curves for the PNJL model at finite volume at the chiral limit and $\mu = 0$. The average Polyakov loop susceptibility $\overline{\chi}_{\Phi\Phi}$ shows a maximum value at a T_d, which is smaller than the chiral temperature T_{ch}, but unlike in the chiral susceptibility, a divergence behavior is not found in the Polyakov loop susceptibility. What is observed is that

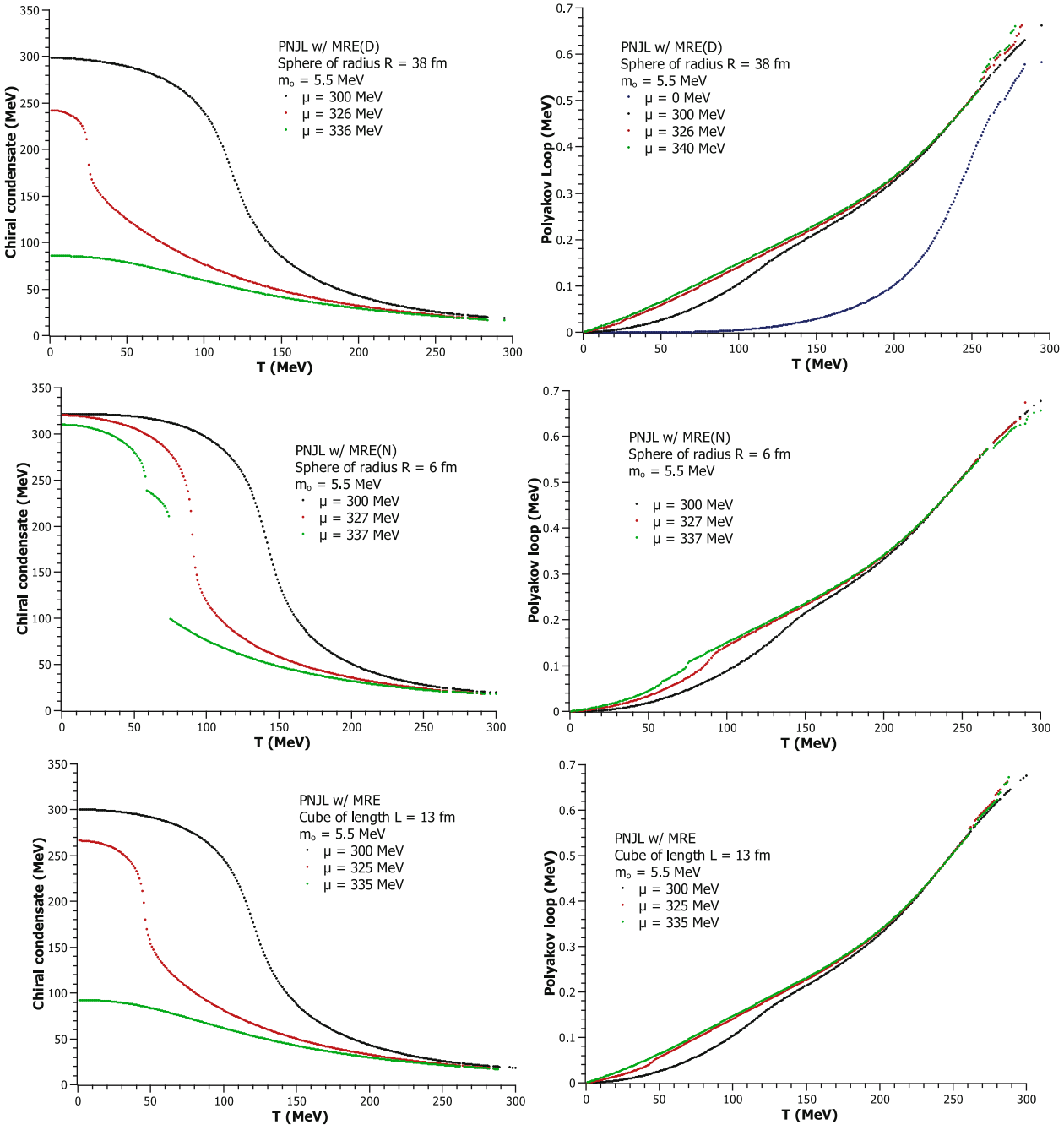

Figure 3: PNJL with MRE_D approximation for a sphere of $R = 38$ fm. Order parameters as a function of the temperature for different values of chemical potential, $\mu = 300$, 326, and 336 MeV. Left, chiral condensate $\langle \bar{q}q \rangle$. Right, Polyakov loop.

the deconfinement temperature is lower than that of a chiral phase transition. The pattern seen in the Polyakov loop susceptibility near the T_{ch} value is similar to that obtained in ref. [2] for the same PNJL model and no volume restrictions. That study found very small differences in the deconfinement temperature for the Polyakov loop susceptibility or the average Polyakov loop susceptibility. Bearing this in mind, in this work, we use $\overline{\chi}_{\Phi\Phi}$.

We are interested in finding, if it exists, a point at which the chiral phase transition takes place. The behavior of order parameters as functions of the temperature for $\mu = 0$ and $m_o = 5.5$ MeV is observed in Figure 5. To better appreciate the relationship of the chiral condensate and the Polyakov loop, the later was normalized at the left side. Top left panel show curves for a sphere of radius $R = 38$ fm using MRE_D; as shown in the bottom left

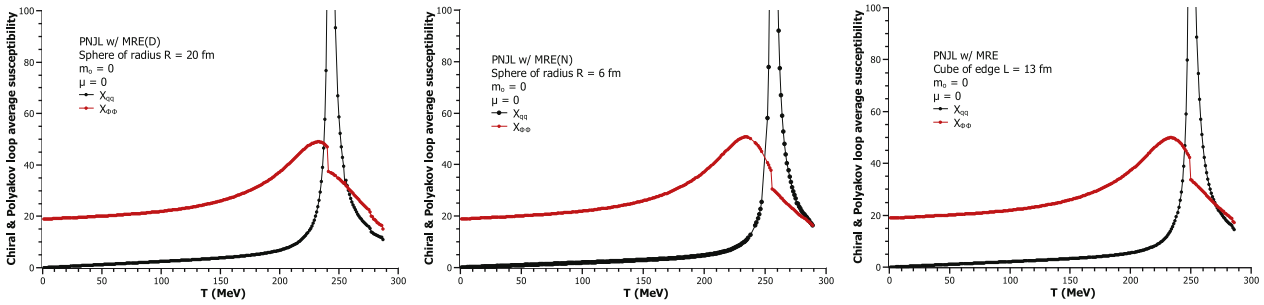

Figure 4: Chiral and average Polyakov loop susceptibilities for the PNJL model and finite volume MRE approximation at the chiral limit and $\mu = 0$. A sphere MRE_D of $R = 20$ fm and a sphere MRE_N of $R = 6$ fm, left and center, respectively. Right, an MRE cube of edge $L = 13$ fm. The chiral temperature T_{ch} corresponds to the peak in chiral susceptibility χ_{MM}. Polyakov loop susceptibilities has been escalated.

panel of the figure, the critical temperature of the Polyakov loop is $T_d \simeq 234$ MeV, and before this value, the chiral condensate tends to be constant. The critical temperature T_c is read at the maximum of the chiral susceptibility. As shown in ref. [26] for the case of PNJL at infinite volume, we found that for the chosen geometries, both critical temperatures are relatively close to each other, being the values of T_{ch} greater than $T = 218$ MeV obtained in ref. [27] for the PNJL model in SU(3) without volume restrictions and the value of $T = 156.5$ MeV using lattice quantum chromodynamics in ref. [28]. Table 2 summarizes these temperatures for a sphere and a cube of different sizes.

The susceptibilities help identifying phase transitions and therefore determining the existence, if any, of the CEP. In order of finding evidence of the existence of this CEP, the behavior of the maximum chiral susceptibility, varying the volume sizes and for values of μ in a wide range, can be studied. Figure 6 shows such curves for cubic geometry and $m_o = 5.5$ MeV. Asymptotic behavior in these curves suggest the existence of a CEP. Then, from Figure 6, it is possible that the CEP exists starting in $L = 11$ fm.

A more detailed analysis of the data was made to find the CEP. Systematical observation of the chiral susceptibility curves were performed for each μ until a divergence is obtained.

Top left panel of Figure 7 shows the evolution of chiral susceptibility when increasing the chemical

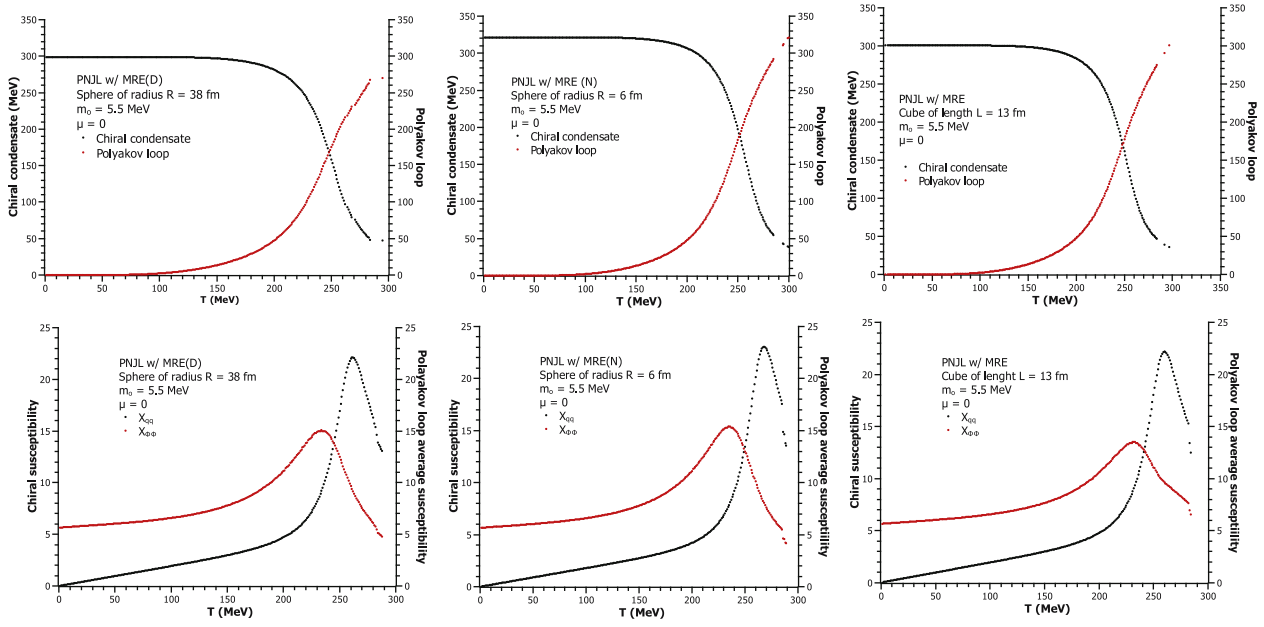

Figure 5: Top, order parameters as function of temperature at $\mu = 0$. Bottom, chiral susceptibility and average Polyakov loop susceptibility $\overline{\chi}_{\Phi\Phi}$. Right, PNJL model with MRE_D approximation for a sphere of $R = 38$ fm. Center, PNJL for a sphere of $R = 6$ fm with MRE_N. Left, a $L = 13$ fm cube.

Table 2: Chiral temperature T_{ch} for $\mu = 0$ in the PNJL model in a finite volume, for different volume sizes and geometries in the chiral limit $m_o = 0$. Bottom for a quark mass of 5.5 MeV

PNJL MRE_D sphere		PNJL MRE_N sphere		PNJL MRE cube	
$m_o = 0$		$m_o = 0$		$m_o = 0$	
R (fm)	T_{ch} (MeV)	R (fm)	T_{ch} (MeV)	L (fm)	T_{ch} (MeV)
50	251	20	257	40	253
20	242	10	257	15	251
10	223	6	256	13	250
6	161	2	247	11	249
		0.9	163	9	247
				5	237

PNJL MRE_D sphere		PNJL MRE_N sphere		PNJL MRE cube	
$m_o = 5.5$ MeV		$m_o = 5.5$ MeV		$m_o = 5.5$ MeV	
R (fm)	T_{ch} (MeV)	R (fm)	T_{ch} (MeV)	L (fm)	T_{ch} (MeV)
50	263	20	269	40	267
40	260	10	269	15	263
38	262	8	269	13	260
20	255	6	268	11	261
10	240	4	267	9	259
6	216	3	265	5	251
		2	260		
		0.9	221		

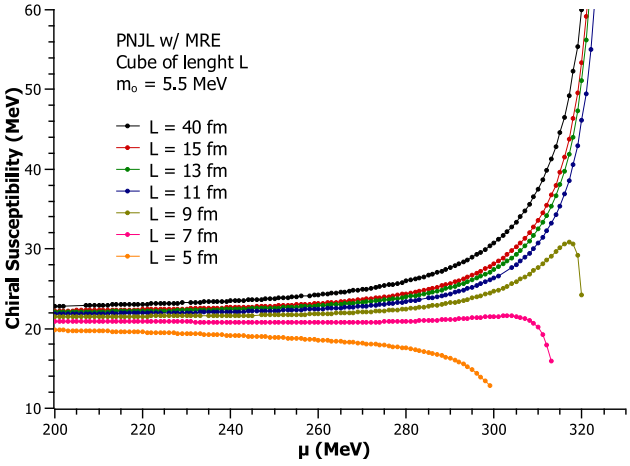

Figure 6: Maximum chiral susceptibility for each value of μ. PNJL model with finite volume using MRE approximation for a cube of lenght L.

potential μ for a finite volume in the PNJL model using MRE_D, in this case, for a sphere of radius $R = 38$ fm. The average susceptibility of the Polyakov loop is shown in the lower left panel. Starting from $\mu = 0$, we found in $\mu = 326$ MeV the first asymptotic behavior for the chiral susceptibility; hence, we propose that the CEP exists for this case. The same asymptotic behavior of Polyakov loop average susceptibility is observed approximately at the

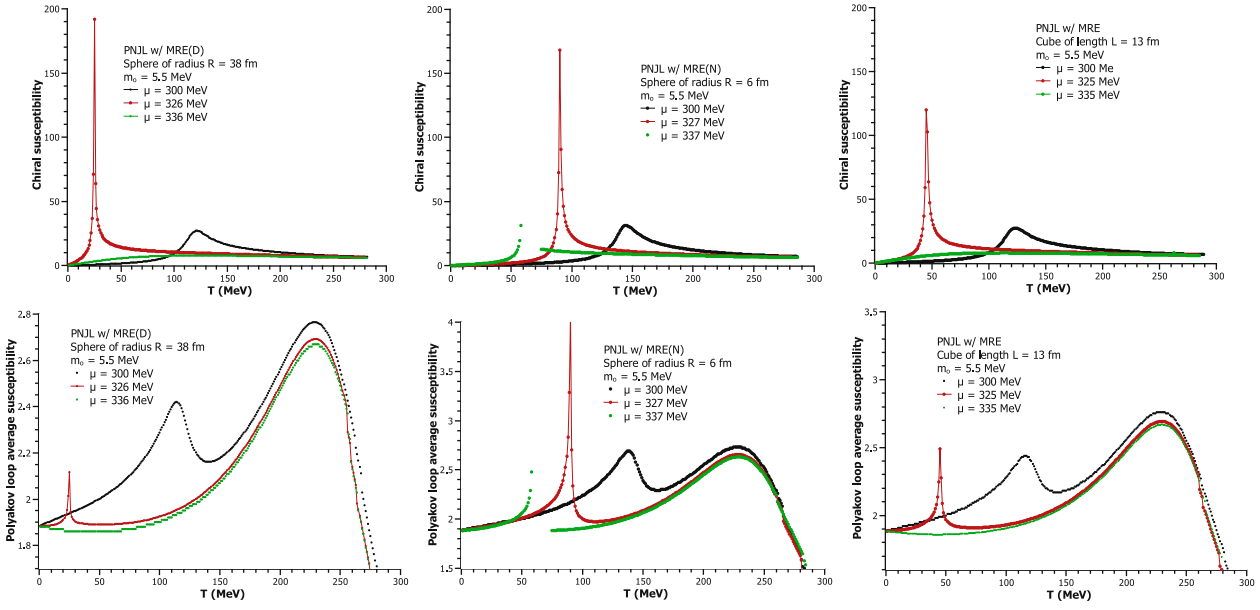

Figure 7: Chiral and Polyakov susceptibilities for different μ values in a finite volume PNJL model using MRE approximation from left to right for a MRE_D sphere of $R = 38$ fm, a MRE_D sphere of $R = 6$ fm, and an MRE cube of $L = 13$ fm. Asymptotic behavior in the susceptibility of the order parameter implies the existence of the CEP.

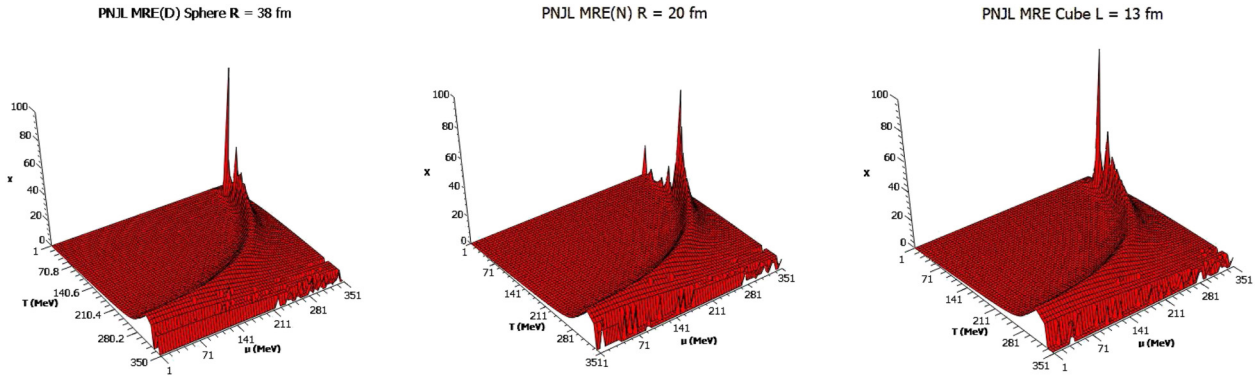

Figure 8: Chiral susceptibility in the $T-\mu$ plane for MRE_D and MRE_N spheres and an MRE cube of $R = 38$, 20 and $L = 13$ fm in the PNJL model for a finite volume with MRE approximation.

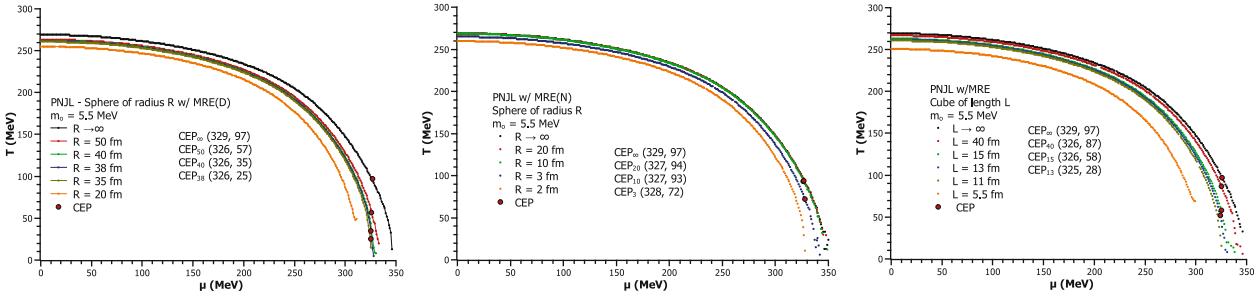

Figure 9: Phase diagram of the PNJL model in a finite volume for sphere with MRE_D (left), MRE_N (right), and cube (bottom) with different volume sizes. CEP is highlighted as a red dot. For R_D under 38 fm, R_N below 3 fm, and L under 13 fm, there is no CEP.

same T. The same analysis is shown in the middle and right panels of the figure for MRE_N in a sphere with $R = 6$ fm and a cube with edge $L = 13$ fm. The CEP appears in $\mu = 327$ and $\mu = 325$ MeV for these cases, respectively.

Figure 8 shows the chiral susceptibility in the $T - \mu$ plane for different volume sizes: MRE_D sphere with $R = 38$ fm, MRE_N sphere with $R = 20$ fm, and MRE cube with edge $L = 13$ fm. The figure shows the expected peak for divergence in susceptibility. This divergence indicates the location of the CEP in the $\mu-T$ plane.

7 Phase diagrams

Figure 9 shows the phase diagram for different sizes of a sphere and a cube. For reference, the phase diagram of PNJL for an infinite volume, that is, without MRE, is shown as a black curve for each geometry. For the PNJL model in a finite volume with MRE approximation, we observe that smaller volume sizes, that is, smaller radius or edge values, correspond to smaller values for the critical temperature. In the same way, the position of the CEP is found each time at increasingly lower temperatures as the volume decreases, until it vanishes. In a sphere with MRE_D, the CEP vanishes for radius values of 35 fm or smaller. Likewise, for a MRE_N sphere, the CEP is found for $R = 3$ fm but not for $R = 2$ fm or smaller. For a cubic geometry, the curve obtained shows almost

Table 3: Critical end point for PNJL model in a finite volume using MRE approximation. Left, sphere of radius R with Dirichlet conditions. Center, for Neumann conditions. Right, for a cube of length L

PNJL MRE_D sphere		PNJL MRE_N sphere		PNJL MRE cube	
R (fm)	CEP (μ, T)	R (fm)	CEP (μ, T)	L (fm)	CEP (μ, T)
$R \gg 1$	(329, 97)	$R \gg 1$	(329, 97)	$L \gg 1$	(329, 97)
50	(326, 57)	20	(327, 94)	40	(326, 87)
40	(326, 35)	10	(327, 93)	15	(326, 58)
38	(326, 25)	8	(327, 92)	13	(325, 28)
<35	—	6	(327, 90)	<11	—
		4	(327, 84)		
		3	(328, 72)		
		<2	—		

no sensitivity to the size of the volume; in this geometry, the CEP exists and is shown for large volumes and gradually decreases in terms of temperature until it vanishes in the cube of $L = 11$ fm. The CEPs found for the different volume sizes and geometries are summarized and shown in Table 3.

8 Discussion

The effects of considering finite volumes were studied using the approximation MRE in the PNJL model in SU (2) in the chiral limit $m_o = 0$ MeV and also for a quark mass $m_o = 5.5$ MeV. Two proposals were explored for the boundary conditions of spherical geometries, as found in ref. [17], namely, MRE_D and MRE_N. An extension was also proposed for studying the effects of cubic geometry in this MRE model; our proposal is rough, and further study can be undertaken to improve the conclusions we made in this work.

In particular, chiral and deconfinement phase transitions in a finite volume were studied. Phase diagrams were obtained and special interest was taken in location, if any, of a CEP. For a spherical shape, it was found that there is a significant difference between Dirichlet and Neumann conditions. In MRE_N, the behavior of the chiral condensate for sizes larger than $R = 6$ fm is almost indistinguishable from a sphere of infinite size. In the case of a MRE_D sphere and a MRE cube, there are notorious differences between infinite volume and volume sizes even as large as $R = 40$ fm and $L = 40$ fm, respectively. This behavior is true for the two quark mass conditions studied, $m_o = 0$ MeV and $m_o = 5.5$ MeV. In particular, we highlight the differences in both the values of the dynamically generated mass M and the chiral symmetry restoration temperatures, as observed in the phase diagrams (Figure 9).

To establish the location of the CEP, we use a divergence criterion in a detailed analysis of the data obtained for the chiral susceptibility as a function of the temperature T, the chemical potential μ, and the volume size used for the different geometries. By studying the $(\mu - T)$ curves generated for χ_{MM}, we define the T-position of a divergence as the smaller value for T, where the slope of the curve is 89° or greater. The CEP coordinates found are given as a position (R, μ, T) for each geometry.

Following these criteria, we found that the CEP exists in MRE_D spheres of radius $R = 38$ fm and larger, MRE_N spheres of radius $R = 3$ fm and larger, and MRE cubes of edge $L = 13$ fm and larger. In other words, we were able to determine a minimum radius for the existence of the CEP for each geometry. Several volume sizes larger than this minimum radius were also studied for each geometry to observe changes, if any, in the location of the CEP.

In all three cases, the temperatures at which the CEP occurs decrease with the size of the volume. The chemical potential values μ also decrease with the size, but its differences are very small compared with decreases in T: our data show decreases of only 4, 3, and 1 MeV for the cube, the MRE_D and MRE_N spheres, respectively.

Although the approximation is limited, it yields results for symmetry restoration temperatures, deconfinement, and/or the location of the CEP consistent with other publications of the NJL/PNJL model with and without volume constraints.

Acknowledgments: This work was partially supported by Consejo Nacional de Ciencia y Tecnología (Conacyt), PhD fellowships and SNI Mexico, and the authors thank the UJED for the facilities granted in computing time.

Funding information: The authors state no funding involved.

Author contributions: All authors have accepted responsibility for the entire content of this manuscript and approved its submission.

Conflict of interest: The authors state no conflict of interest.

Data availability statement: Data sharing is not applicable to this article as no datasets were generated or analysed during the current study.

References

[1] Fukushima K, Ruggieri M, Gatto R. Chiral magnetic effect in the Polyakov-Nambu–Jona–Lasinio model. Phys Rev. 2010;81(11):114031.

[2] Sasaki C, Friman B, Redlich K. Susceptibilities and the phase structure of a Chiral model with Polyakov loops. Phys Rev. 2007;75(7):074013–17.

[3] Xu F, Huang M. The chiral and deconfinement phase transitions. Open Phys. 2012;10(6):1357–60.

[4] Morones-Ibarra JR, Mata-Carrizal NB, Valbuena-Ordóñez E, Garza-Aguirre AJ. Dependence of the crossover zone on the regularization method in the two-flavor Nambu-ona-Lasinio model. Open Phys. 2020;18(1):089–103.

[5] Morones-Ibarra JR, Enriquez-Perez-Gavilan A, Rodriguez AIH, Flores-Baez FV, Mata-Carrizalez NB, Ordoñez EV. Chiral symmetry restoration and the critical end point in QCD. Open Phys. 2017;15(1):1039–44.

[6] Cui Y-Q, Pan Z-L. Studies on proper time regularization and the QCD chiral phase transition. Modern Phys Lett A. 2019;34(1):1950003–9.
[7] Cui Z-F, Hou F-Y, Shi Y-M, Wang Y-L, Zong H-S. Progress in vacuum susceptibilities and their applications to the chiral phase transition of QCD. Ann Phys (NY). 2015;358:172–205.
[8] Stephanov MA. Qcd phase diagram and the critical point. Int J Mod Phys A. 2005;20(19):4387–92.
[9] Bazavov A, Bhattacharya T, Cheng M, DeTar C, Ding H-T, Gottlieb S, et al. Chiral and deconfinement aspects of the QCD transition. Phys Rev. 2012;85(5):054503.
[10] Schmitt A. Dense matter in compact stars – A pedagogical introduction. 2010. arXiv [astro-ph.SR].
[11] Costa P, Ruivo MC, de Sousa CA. Thermodynamics and critical behavior in the Nambu–Jona–Lasinio model of QCD. Phys Rev. 2008;77(9):096001.
[12] Wang Q-W, Xia Y, Zong H-S. Nambu–Jona–Lasinio model with proper time regularization in a finite volume. Modern Phys Lett A. 2018;33(39):1850232.
[13] Fukushima K. Phase diagrams in the three-flavor Nambu–Jona–Lasinio model with the Polyakov loop. Phys Rev D. 2008;77(11):114028–17.
[14] Ayala A, Hernández L, Loewe M, Villavicencio C. QCD phase diagram in a magnetized medium from the chiral symmetry perspective: The linear sigma model with quarks and the Nambu–Jona–Lasinio model effective descriptions. Eur Phys J A. 2021;57(7):234.
[15] Fraga E, Kodama T, Palhares L, Sorensen P. Finite-size effects and the search for the critical endpoint of QCD, 2011. Proceedings of Science, PoS FACESQCD, 017, 2010, doi: 10.22323/1.117.0017 [arXiv:1106.3887[hep-ph]].
[16] Balian R, Bloch C. Distribution of eigenfrequencies for the wave equation in a finite domain. Ann Phys (NY). 1970;60(2):401–47.
[17] Kiriyama O, Kodama T, Koide T. Finite-size effects on the QCD phase diagram. 2006. arXiv [hep-ph].
[18] He YB, Chao WQ, Gao CS, Li XQ Cold strangelets formation with finite size effects in high energy heavy-ion collisions. Phys Rev C Nuclear Phys. 1996;54(2):857–65.
[19] Kiriyama O. Colour-superconducting strangelets in the Nambu–Jona–Lasinio model. Phys Rev D. 2005;72(5):054009–10.
[20] Madsen J. Shell model versus liquid drop model for strangelets. Phys Rev D Particles Fields. 1994:50(5):3328–31. Available from: doi: 10.1103/physrevd.50.3328.
[21] Zhao Y-P, Yin P-L, Yu Z-H, Zong H-S. Finite volume effects on chiral phase transition and pseudoscalar mesons properties from the Polyakov-Nambu–Jona–Lasinio model. Nucl Phys B. 2020;952(114919):114919.
[22] Grunfeld AG, Lugones G. Finite size effects in strongly interacting matter at zero chemical potential from polyakov loop Nambu–Jona–Lasinio model in the light of lattice data. Eur Phys J C. 2018;78(8):640–12.
[23] Bhattacharyya A, Ghosh SK, Ray R, Saha K, Upadhaya S. Polyakov-Nambu–Jona–Lasinio model in finite volumes. Europhys Lett. 2016;116(5):52001–7.
[24] Valbuena-Ordóñez E, Mata-Carrizal NB, Garza-Aguirre AJ, Morones-Ibarra JR. Influence of the effective potential on the crossover width in the two flavor Polyakov-Nambu–Jona–Lasinio model. Adv High Energy Phys. 2020;2020:1–14.
[25] Blanquier E. Standard particles in the SU(3) Nambu–Jona–Lasinio model and the Polyakov-NJL model. J Phys G Nucl Part Phys. 2011;38(10):105003.
[26] Fukushima K. Chiral effective model with the polyakov loop. Phys Lett B. 2004;591(3–4):277–84.
[27] Blaschke D, Friesen AV, Kalinovsky YL, Radzhabov A. Chiral phase transition and kaon-to-pion ratios in the entanglement SU(3) PNJL model. Eur Phys J Spec Top. 2020;229(22–23):3517–36.
[28] Bazavov A, Ding H-T, Hegde P, Kaczmarek O, Karsch F, Karthik N, et al. Chiral crossover in QCD at zero and non-zero chemical potentials. Phys Lett B. 2019;795:15–21.
[29] Ratti C, Thaler MA, Weise W. Phases of QCD: Lattice thermodynamics and a field theoretical model. Phys Rev D. 2006;73(1):014019–10.
[30] Roessner S, Ratti C, Weise W. Polyakov loop, diquarks and the two-flavour phase diagram. Phys Rev D. 2007;75(3):034007.
[31] Holland K, Wiese U-J. The center symmetry and its spontaneous breakdown at high temperatures. At The Frontier of Particle Physics. April 2001. 1909–44. doi: 10.1142/9789812810458_0040.
[32] Pepe M. Confinement and the center of the gauge group. Nuclear Phys B Proc Suppl. 2006;153(1):207–14.
[33] Buballa M. NJL-model analysis of dense quark matter. Phys Rep. 2005;407(4–6):205–376.
[34] Kohyama H, Kimura D, Inagaki T. Regularization dependence on phase diagram in Nambu–Jona–Lasinio model. Nucl Phys B. 2015;896:682–715.
[35] Klevansky SP. The Nambu–Jona–Lasinio model of quantum chromodynamics. Rev Modern Phys. 1992;64(3):649–708.
[36] Fujii H. Scalar density fluctuation at critical end point in NJL model. Phys Rev D. 2003;67(9):094018–7.